

SUPPORTING INFORMATION

Post-synthetic modification of Covalent Organic Frameworks with active Manganese centers for the electrocatalytic CO₂ reduction in water.

Elena Gala,^{a,b,φ} Geyla C. Dubed Bandomo,^{c,φ} Mattia Vettori,^c Sergio Royuela,^d Marcos Martínez-Fernández,^a José I. Martínez,^e Elena Salagre,^{f,g} Enrique G. Michel,^{f,g} Félix Zamora,^{d,g,h} Julio Lloret,^{c,i} and José L. Segura^{a*}*

E. Gala, M. Martínez-Fernández, J.L. Segura

^aDepartamento de Química Orgánica I, Facultad de CC. Químicas, Universidad Complutense de Madrid, 28040 Madrid, Spain.

E-mail: segura@ucm.es

E. Gala

^bChemical and Environmental Technology Department, Rey Juan Carlos University, Móstoles, 28933, Spain.

G.C. Dubed Bandomo, M. Vettori, J. Lloret-Fillol

^cInstitute of Chemical Research of Catalonia (ICIQ), The Barcelona Institute of Science and Technology, Tarragona 43007, Spain

Email: jlloret@iciq.es

S. Royuela, F. Zamora

^dDepartamento de Inorgánica, Facultad de Ciencias, Universidad Autónoma de Madrid, Campus de Cantoblanco - Crta. Colmenar, Madrid 28049, Spain

J.I. Martínez

^eDepartamento de Materiales de baja dimensionalidad, Instituto de Ciencia de Materiales de Madrid (ICMM-CSIC), 28049 Madrid, Spain

E. Salagre, E. G. Michel

^fDepartamento de Física de la Materia Condensada, Universidad Autónoma de Madrid, 28049, Madrid, Spain

E. Salagre, E. G. Michel, F. Zamora

^gCondensed Matter Physics Center (IFIMAC), Universidad Autónoma de Madrid, 28049, Madrid, Spain.

F. Zamora

^hInstitute for Advanced Research in Chemical Sciences (IAdChem). Universidad Autónoma de Madrid, Campus de Cantoblanco. Madrid 28049, Spain

J. Lloret-Fillol

ⁱCatalan Institution for Research and Advanced Studies (ICREA), Barcelona 08010, Spain

^φElena Gala and Geyla C. Dubed Bandomo contributed equally to this work

Index

1. GENERAL METHODS AND MATERIALS.....	3
2. CHARACTERIZATION TECHNIQUES.....	4
3. SYNTHESIS.....	6
4. NMR SPECTRA.....	8
5. COMPARATIVE FTIR AND UV-VIS SPECTRA.....	10
6. PORE SIZE DISTRIBUTION OF [HC≡C] _{0.17} -TPB-DMTP-COF, TERPY-COF AND Mn@TERPY-COF.....	11
7. MICROSCOPY IMAGES.....	13
8. THERMOGRAVIMETRIC ANALYSIS (TGA) OF TERPY-COF AND Mn@TERPY-COF.....	17
9. POWDER X-RAY DIFFRACTION OF TERPY-COF AND Mn@TERPY-COF.....	18
10. XPS SPECTRA.....	19
11. CPE EXPERIMENTS.....	22
12. CV OF Mn@TERPY-COF NT.....	23
13. ATR SPECTRA OF TERPY-COF AND Mn@TERPY-COF.....	24
14. REFERENCES.....	25

1. GENERAL METHODS AND MATERIALS

The following reagents were commercially available and were used as received: *o*-DCB, *n*-BuOH, acetic acid, anhydrous DMF and CuI. **DMTA**,¹ **BPTA**,¹ **TAPB**¹ and 4'-azido-2,2':6',2''-terpyridine **1**² were prepared according to reported procedures. Air-sensitive reactions were performed under argon atmosphere. TLC analyses were performed using silica gel (Kieselgel 60 F254, Macherey–Nagel) and spots were visualized under UV light. Column chromatography was carried out with silica gel 60 (0.04-0.06 mm, Scharlau) columns, using the eluent reported in each case.

Computational Methods.

Molecular fragments. As starting point, the theoretical investigation of the molecular fragments involved in the formation of the different COF-systems was carried out by density functional theory (DFT) as implemented in the Gaussian 16 C.01 atomistic simulation package.³ The M062X functional⁴ was adopted to account for the exchange-correlation energy, and the 6–311+G(d, p) basis set for the all-electron modelling of all the atoms involved^{5–7} All geometric parameters were allowed to vary independently, and frequency calculations confirmed the calculated geometries as minima.

Periodic calculations. Periodic boundary conditions were applied for simultaneous structure + cell optimizations of various stacked 3D layered COF model systems based on their canonical 2D network structures. QUANTUM ESPRESSO plane-wave DFT code⁸ was used to construct optimized 2D networks with the GGA-PBE functional⁹ accounting for exchange-correlation effects. Grimme DFT-D3 correction¹⁰ was used to include dispersion forces. Ultra-soft pseudopotentials^{11,12} were adopted to model ion-electron interactions, and Brillouin zones were sampled using $[2 \times 2 \times 1]$ and $[2 \times 2 \times 8]$ Monkhorst-Pack grids¹³ for 2D layers and 3D crystals, respectively. Full structure + cell optimizations involved atomic relaxations until forces on any atom were below $0.02 \text{ eV } \text{Å}^{-1}$, including interlayer distances. Both eclipsed (AA) and staggered (AB) configurations were analyzed for crystal-bulk models.

Calculation of the reaction paths. The calculation of all the intermediates participating in the proposed mechanisms toward the formate anion and CO evolution were conducted by using the Gaussian 16 C.01 atomistic simulation package.³ Geometry optimizations utilized the M062X exchange-correlation functional⁴ and the 6–311+G(d, p) basis set for all the atoms involved.⁷ Vibrational frequency calculations characterized each stationary point and included zero-point energy (ZPE) corrections and entropic contribution at 300 K to obtain the Gibbs free energies for each reaction step. We have accounted for the influence of bias on all states associated with an electron in the electrode by shifting the energy of these states by $-eU$, where e is the electron charge and U represents the electrode potential.^{14,15} We have adopted as reference electrode in redox reactions the Saturated Calomel Electrode (SCE). A tight convergence criterion (10^{-12} a.u.) was established, and the solvent water was considered using the integral equation formalism polarizable continuum model (IEF-PCM).¹⁶

2. CHARACTERIZATION TECHNIQUES

IR spectra of [HC≡C]_{0.17}-TPB-DMTP-COF and Terpy-COF were recorded on a Bruker TENSOR 27 on a diamond plate (ATR) and they are reported in wavenumbers (cm⁻¹). **NMR**: ¹H and ¹³C NMR spectra in solution were recorded using Bruker DPX 300MHz or Bruker AVIII 300MHz BACS-60 systems at room temperature. Solid state ¹³C cross-polarized magic angle spinning solid-state NMR (¹³C CP/MAS NMR) were recorded on a 400 MHz spectrometer Wide Bore (probe: Hv /X BB of 4 mm). The sample rotation frequency was 12 kHz and a 2.5 mm ZrO₂ rotor was used. **N₂ (77 K) sorption isotherms** were analyzed using a Micromeritics Tristar 3000. Samples were previously activated under high vacuum at 120 °C. **Scanning electron microscopy (SEM)** was used to study the morphology and shape of the COFs. The images were taken on a JEOL JSM 7600F scanning electron microscope. **UV-Vis** spectra were recorded on a Varian Cary 50 UV-vis spectrophotometer. For these UV-vis data acquisition, COFs were suspended and exfoliated in a HCl acidulated THF:H₂O 7:3 solution.

Electrochemistry:

Materials and reagents. Multi-walled Carbon Nanotubes (MWCNTs) (purity 95%) and FTO plates were purchased from Sigma-Aldrich. K₂SO₄, K₂B₄O₇, TBAPF₆, Nafion, acetonitrile and other chemicals and solvents were purchased from commercial suppliers and used as received.

Cyclic Voltammetry. Working electrode: Glassy carbon (GC) electrodes (99.9995% trace metal basis, purchased from Bio-Logic) were polished with diamond paste and alumina (3 and 1 μm for 60 seconds each), thoroughly rinsed and sonicated in water and acetone, and dried before functionalization. Working electrodes (GC, 0.0717 cm²) were prepared by drop casting 10 μL of an ink containing the catalyst and MWCNTs (NT) (1 mg) dispersed in CH₃CN and Nafion 5% in water (1:1, 200 μL) and let dry under dark.

Electrochemical measurements were performed using a Biologic potentiostat/galvanostat with a glass cell in the dark. The three-electrodes setup consisted of a working electrode, a Pt wire counter electrode, and a reference electrode. The reference electrode used in water was SCE (3.5 M KCl solution), while in CH₃CN was Ag wire, a pseudo reference calibrated with Fc⁺/Fc vs a freshly clean glassy carbon electrode before and after experiments. All experiments were performed in water (0.2 M K₂SO₄/0.1 M K₂B₄O₇) or CH₃CN (0.2 M TBAPF₆) electrolyte under Ar or CO₂ atmosphere at 25 °C. The cell was purged for 10 minutes before each experiment. The pH was measured using a CyberScan pH510. Ohmic drop was compensated using the positive feedback compensation implemented in the instrument.

Controlled Potential Electrolysis (CPE). For CPE experiments, an H-type electrochemical cell was used, in which the counter electrode was a Pt wire immersed in a bridge tube containing electrolyte solution and separated from the cathodic compartment by a ceramic frit. Working electrodes were prepared by spraying onto carbon paper (CP, Freudenberg H23C6) an ink containing the catalyst and MWCNTs (NT) dispersed in EtOH and Nafion 5% in water (1:1, 200 μL) and let dry under dark, we employed SCE electrode as reference. To

saturate with Ar or CO₂, a constant gas flow (30 ml·min⁻¹, fixed with a mass-flow controller, Alicat®) was continuously passed over the solution and on-line analyzed with gas chromatography every 10 minutes. An Agilent 490 micro gas chromatograph equipped with a thermal conductivity detector and a Molesieve 5Å column was calibrated with different H₂/He/CO/CH₄ mixtures of known composition. The products formed during the reaction in liquid phases were analyzed by ¹H-NMR recorded on Bruker AV400 and AV500 spectrometers using standard conditions (300 K) and maleic acid as analytical standard. The Faradaic Yield has been calculated by the following equation:

$$FY(\%) = ne \cdot (mol_{product}/mol_e) \cdot 100$$

Where: ne is the number of electrons of the redox transformation (2 for H₂, CO and HCO₂⁻) and $mol_{product}$ and mol_e are the number of moles of product generated and moles of electrons consumed in the CPE at a given time. $mol_{product}$ was determined by integrating the chromatogram areas, considering the flow of gas and Δt between each measurement. mol_e was determined by integrating the charge.

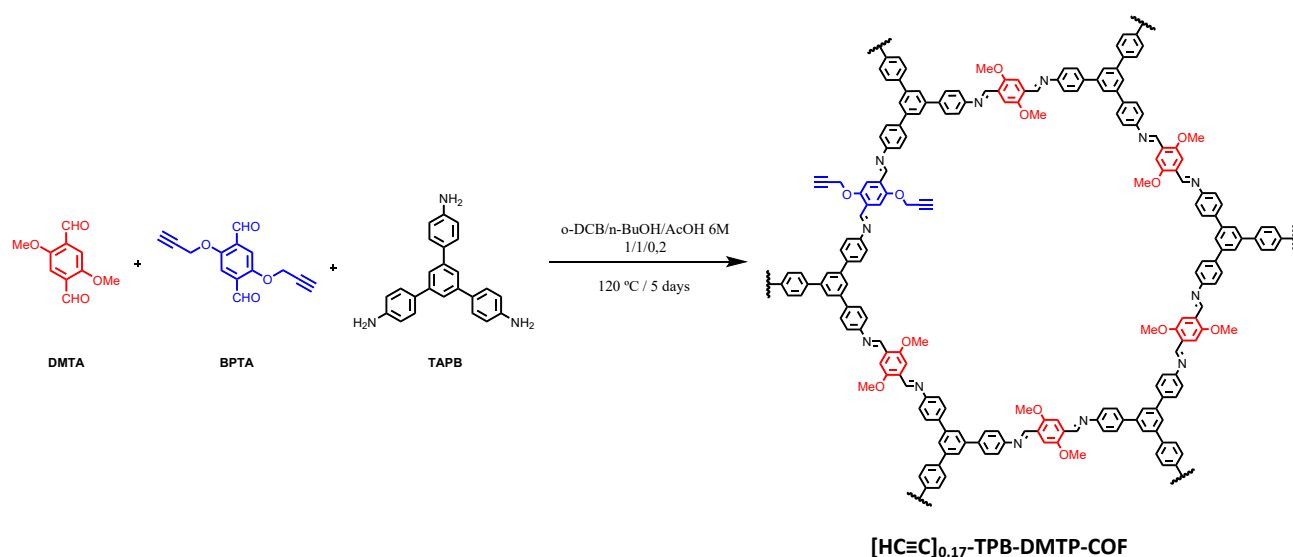
Spectroelectrochemistry. The **Mn@Terpy-COF|NT** membrane film was deposited over the Si prism and was electrically connected and pressed by a Titanium electrode (tip $d=0.25$ cm) to produce the working electrode into a homemade ATR IR spectroelectrochemical cell (fill volume of 4 mL). A Ag wire 0.2 M TBAPF₆/CH₃CN was used as reference electrode. The counter electrode was a Pt wire immersed in a bridge tube containing electrolyte solution and separated from the cathodic compartment by a ceramic frit. To ensure saturation with Ar, a constant gas flow was continuously passed over the solution. All measurements were carried out at room temperature. A total of 128 scans were co-added for a spectrum. The spectral region was set to a range from 400 to 4000 cm⁻¹. The resolution of the spectra was 4 cm⁻¹. ATR-IR spectra of **Mn@Terpy-COF** and materials containing Mn@Terpy-COF were recorded on a Nicolet iS50 spectrometer using ATR accessory.

X-ray photoelectron spectroscopy (XPS) experiments were performed in an ultrahigh vacuum (UHV) chamber. Mg K α radiation excites core level photoelectrons, which are detected using a Specs Phoibos-150 electron analyzer with a constant pass energy of 20 eV. The axis of the electron analyzer was fixed and coincided with the surface normal. The binding energies of the core levels were calibrated against the reference binding energies of C 1s and Au 4f in contact with the sample. The line shape of the core levels was fitted using a Shirley background and asymmetric singlet pseudo-Voigt functions. The fit was optimized using a Levenberg–Marquardt algorithm with a routine running in IGOR Pro (WaveMatrix Inc.)¹⁷. The quality of the fit was assessed by a reliability factor, the normalized χ^2

3. SYNTHESIS

Synthesis of $[\text{HC}\equiv\text{C}]_{0.17}\text{-TPB-DMTP-COF}^1$

Following the reported procedure, **DMTA** (68.0 mg, 0.35 mmol), **BPTA** (22.7 mg, 0.07 mmol) and **TAPB** (98.3 mg, 0.28 mmol) were suspended in a mixture of *o*-DCB/*n*-Butanol (2 mL/2 mL) and acetic acid (6 M, 0.35 mL). The mixture was briefly sonicated and the Pyrex vessel was degassed via three freeze-pump-thaw cycles, flame sealed and heated at 120 °C for 3 days. The precipitate was collected by filtration and further Soxhlet extracted. The resulting solid was dried at 90 °C under vacuum overnight to give 146 mg (84 %) of a yellow solid. ^{13}C CP/MAS-NMR, δ (ppm): 154.8, 148.6, 140.8, 128.8, 123.8, 122.6, 113.2, 109.5, 79.2, 54.0. FTIR (ATR), ν (cm^{-1}): 2950, 1684, 1593, 1457, 1406, 1285, 1209, 1142, 1034, 827, 688.



Scheme S1. Synthesis of $[\text{HC}\equiv\text{C}]_{0.17}\text{-TPB-DMTP-COF}$.

Synthesis of Terpy-COF

$[\text{HC}\equiv\text{C}]_{0.17}\text{-TPB-DMTP-COF}$ (104 mg) was suspended in anhydrous DMF (2.4 mL) under argon atmosphere. Then, and in this order, *N,N*-diisopropylethylamine (DIPEA, 25.7 μL), CuI (8 mg) and the terpyridine azide **1** (24.4 mg) were added to the reaction mixture. Finally, additional 2.4 mL of anhydrous DMF were added and the reaction was left to react at room temperature overnight. The solid was collected by filtration, washed four times alternating acetonitrile and THF and dried at 90 °C under vacuum overnight. The desired product, **Terpy-COF**, was obtained as a yellow solid. ^{13}C CP/MAS-NMR, δ (ppm): 154.6, 148.9, 141.0, 128.5, 123.6, 122.5, 117.4, 109.3, 56.1, 53.8. FTIR (ATR), ν (cm^{-1}): 2941, 1593, 1506, 1464, 1412, 1289, 1210, 1039, 828, 696.

Synthesis of Mn@Terpy-COF

To a **Terpy-COF** suspension in Et₂O (10 mL), Mn(CO)₅Br (1.1 equi. of terp) was added and then refluxed for 4 h. The resulting solid was collected by filtration, and the dark brown solid was washed profusely with Et₂O (3 × 10 mL) until the supernatant was colorless. The solid was dried under vacuum at room temperature and kept under inert atmosphere. *Because of the light-sensitive nature of Mn complex, all reaction steps were performed with minimal exposure to ambient light.*

4. NMR SPECTRA

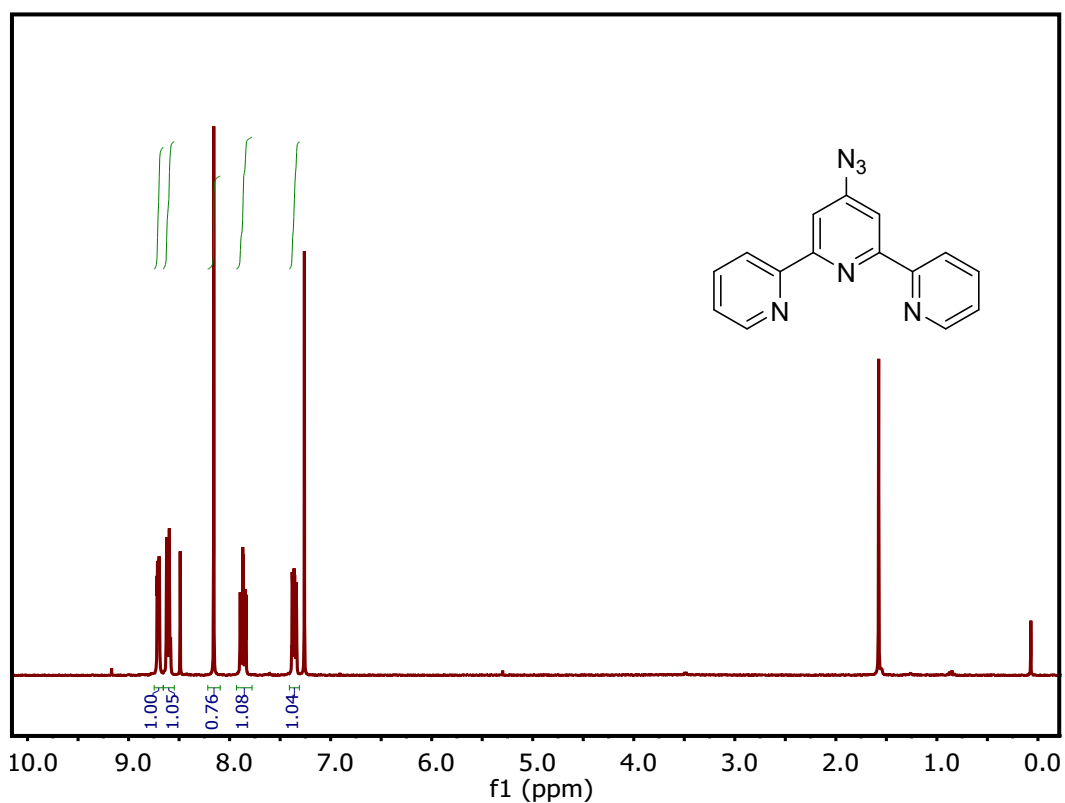


Figure S1. ¹H-NMR spectrum of 4'-azido-2,2':6',2''-terpyridine 1.

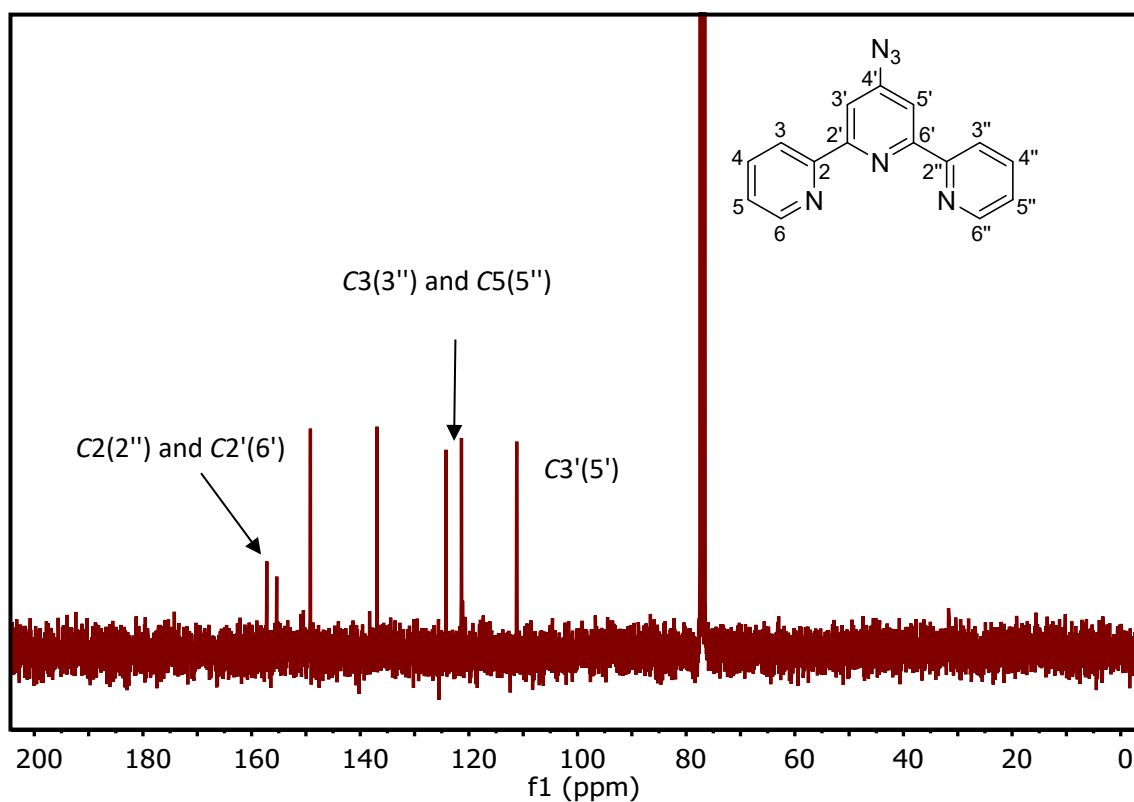


Figure S2. ¹³C-NMR spectrum of 4'-azido-2,2':6',2''-terpyridine 1.

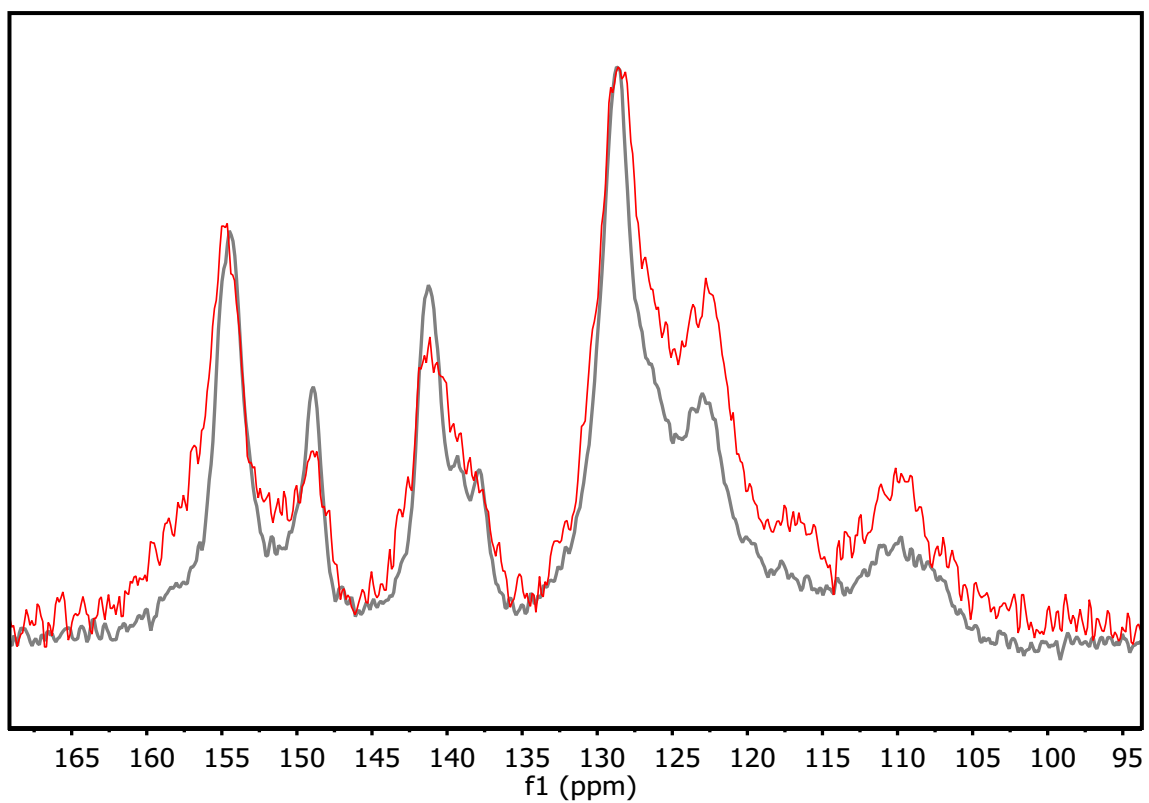


Figure S3. Superposed spectra of aromatic region of ¹³C-NMR of [HC≡C]_{0.17}-TPB-DMTP-COF (black) and Terpy-COF (red).

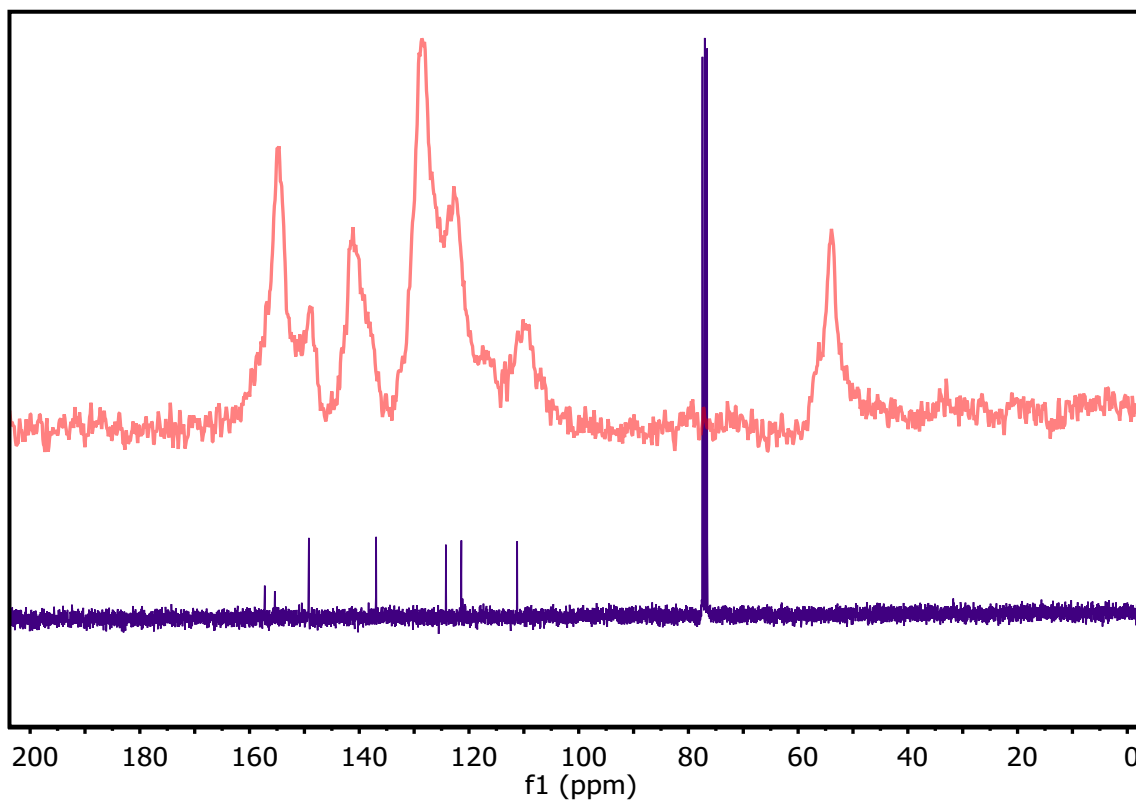


Figure S4. Superposed spectra ¹³C-NMR of Terpy-COF (red) and 4'-azido-2,2':6',2''-terpyridine 1 (purple).

5. COMPARATIVE FTIR AND UV-VIS SPECTRA

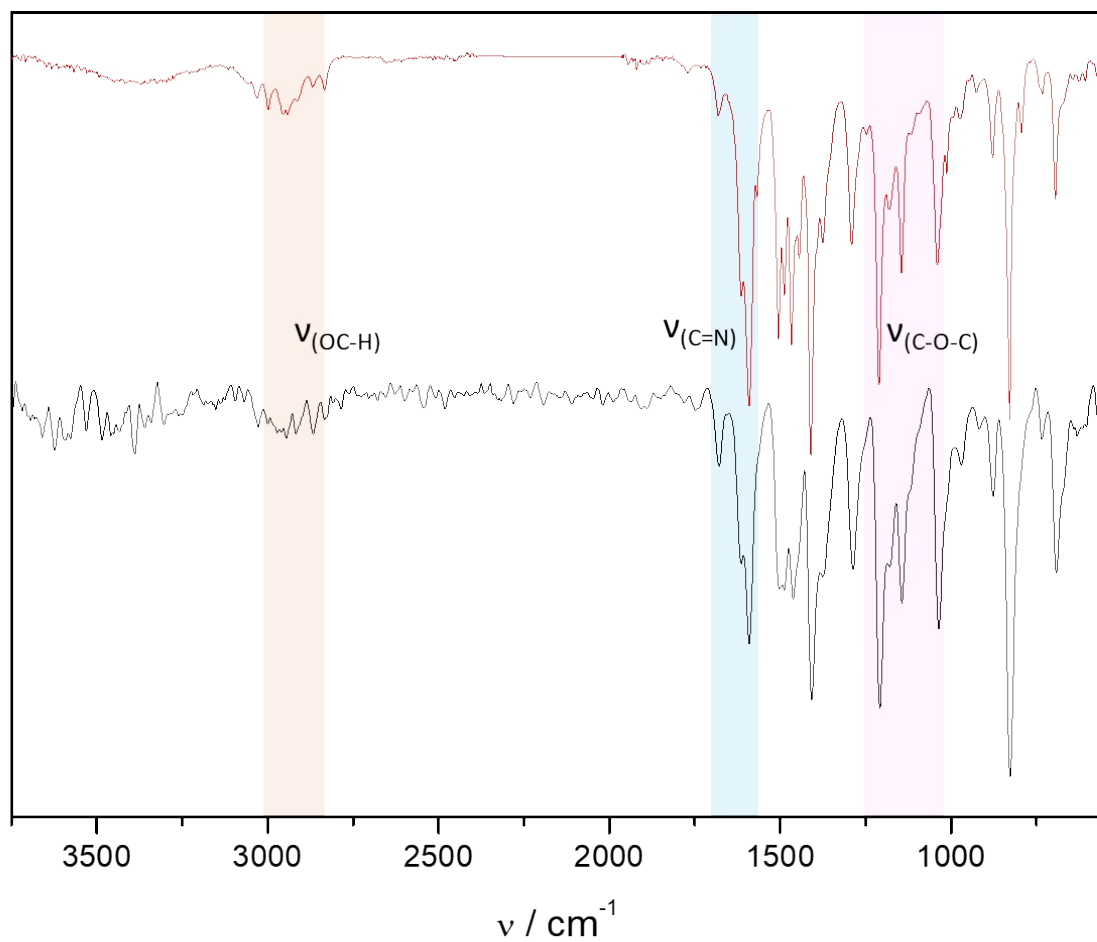


Figure S5. Comparative FTIR spectra of $[\text{HC}\equiv\text{C}]_{0.17}\text{-TPB-DMTP-COF}$ (black) and Terpy-COF (red).

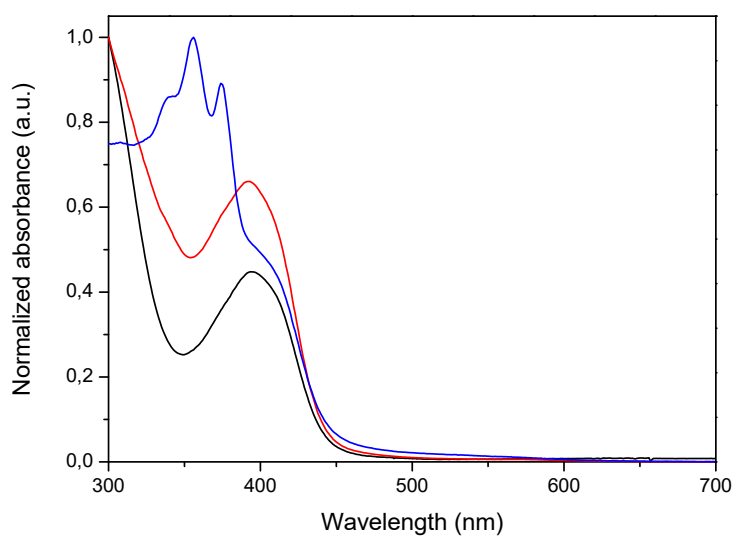
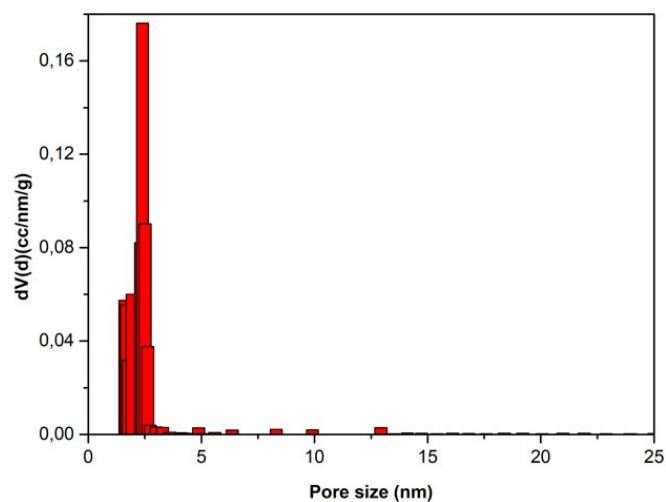


Figure S6. Normalized comparative UV-Vis absorption spectra of $[\text{HC}\equiv\text{C}]_{0.17}\text{-TPB-DMTP-COF}$ (black), Terpy-COF (red) and Mn@Terpy-COF (blue).

6. PORE SIZE DISTRIBUTION OF $[\text{HC}\equiv\text{C}]_{0.17}\text{-TPB-DMTP-COF}$, TERPY-COF AND Mn@TERPY-COF



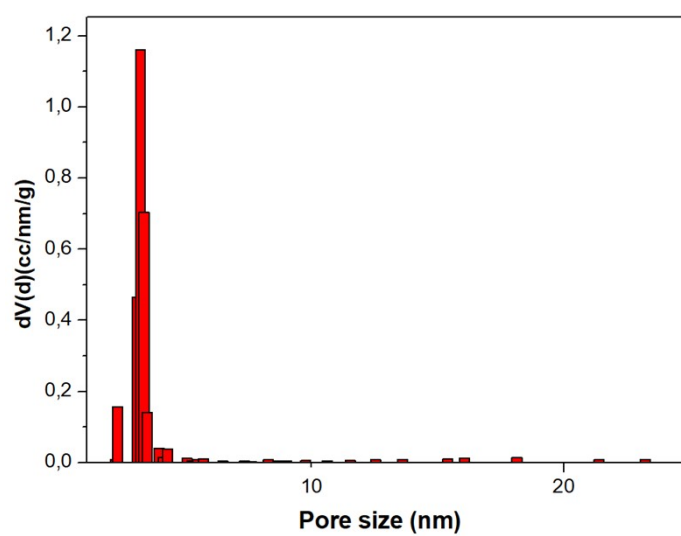
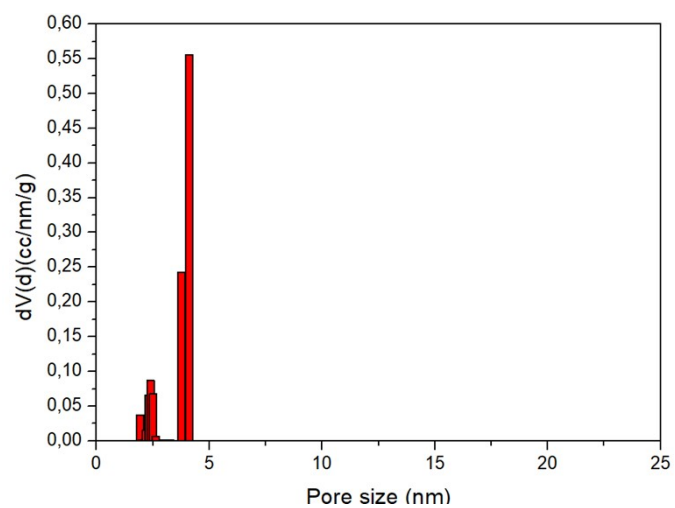


Figure S7. Pore size distribution of [HC≡C]_{0.17}-TPB-DMTP-COF (top), Terpy-COF (middle) and Mn@Terpy-COF (down).

7. MICROSCOPY IMAGES

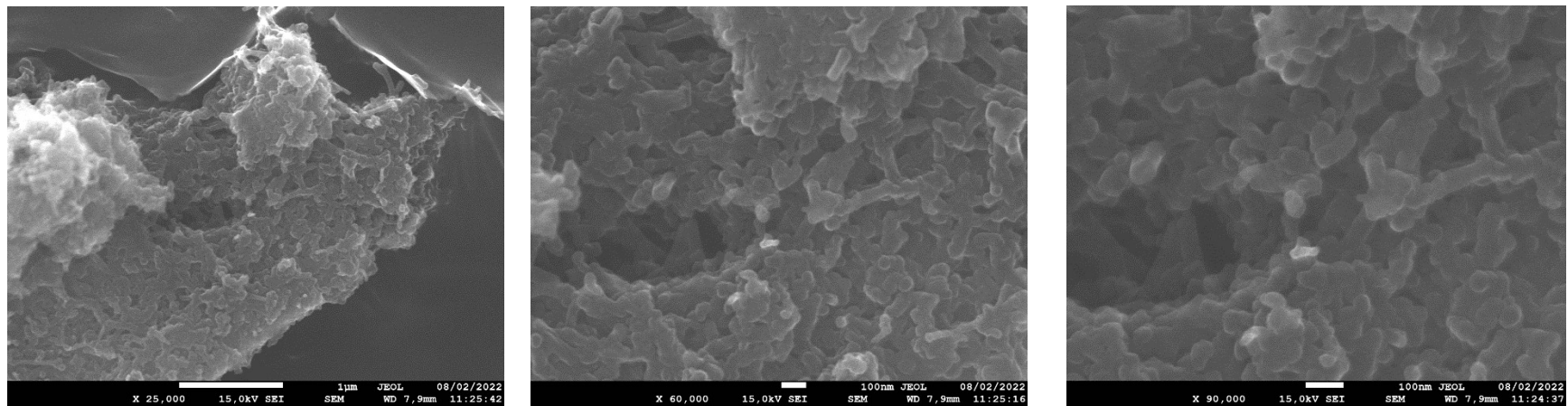


Figure S8. SEM images of [HC≡C]_{0.17}-TPB-DMTP-COF.

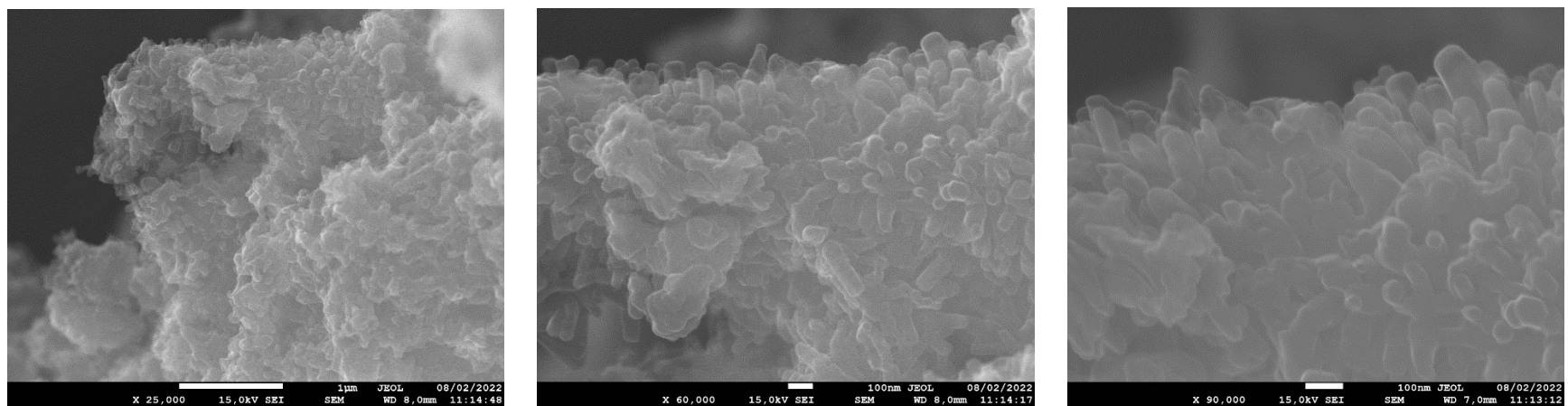


Figure S9. SEM images of Terpy-COF

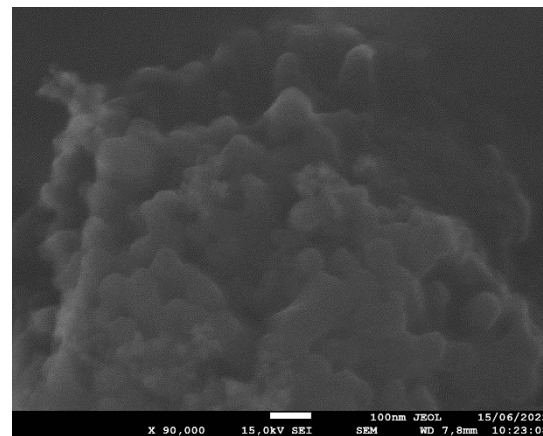
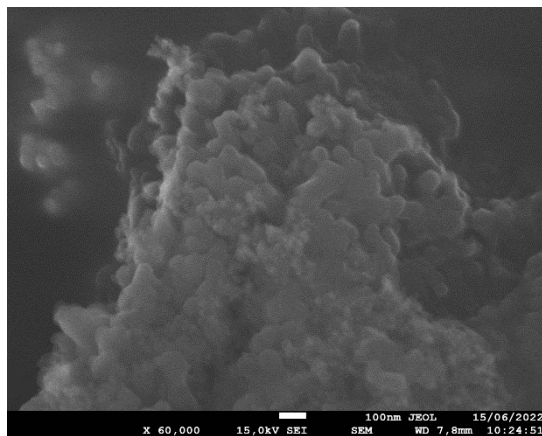
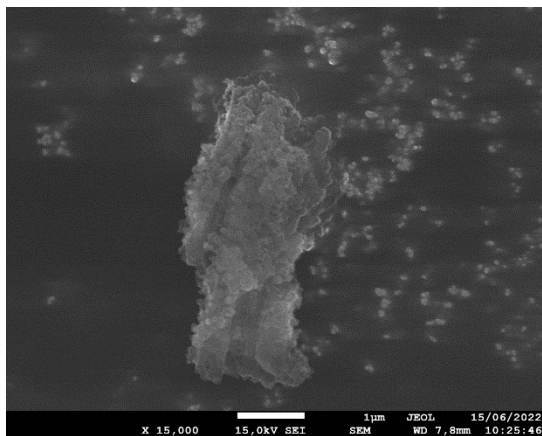


Figure S10. SEM images of Mn@Terpy-COF

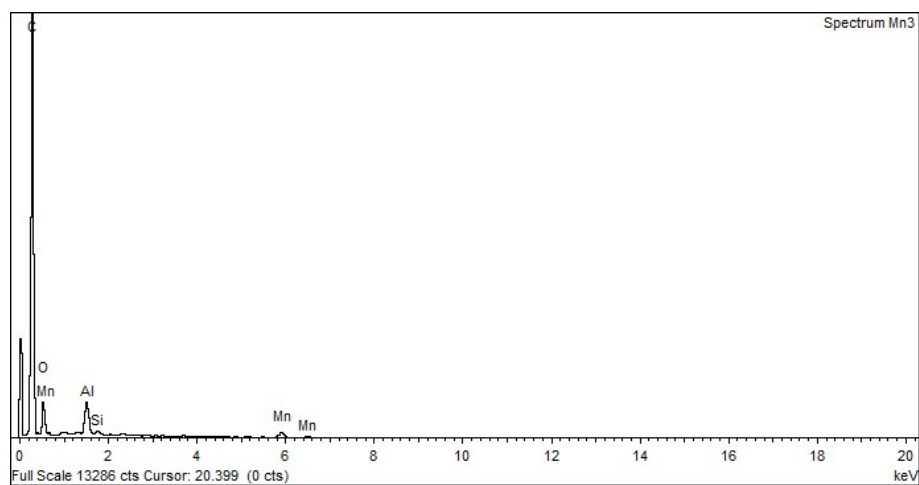


Figure S11. EDS of Mn@Terpy-COF of the fragment showed in figure S10 (right)

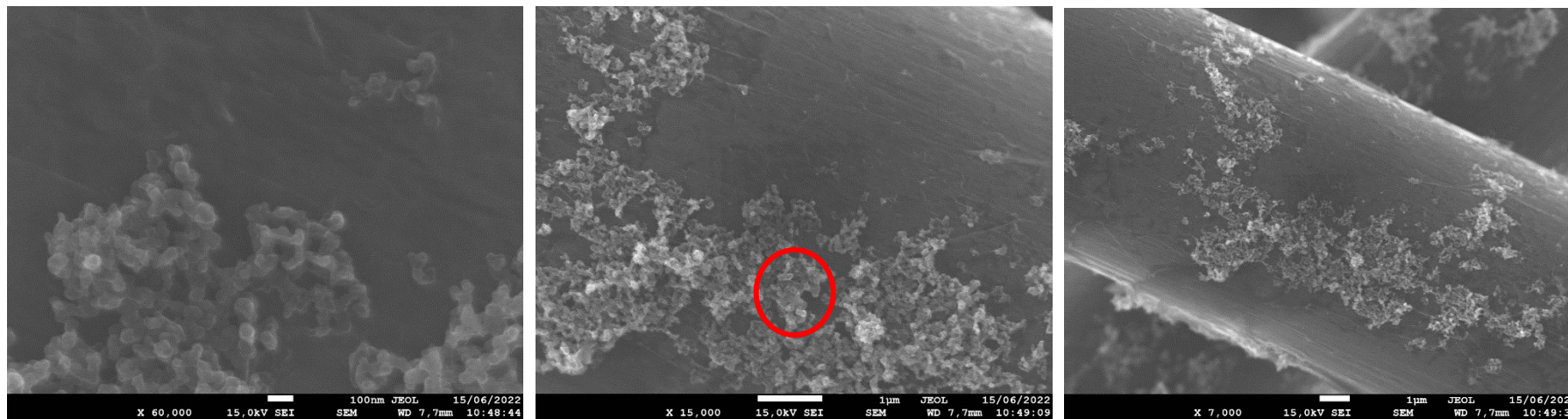
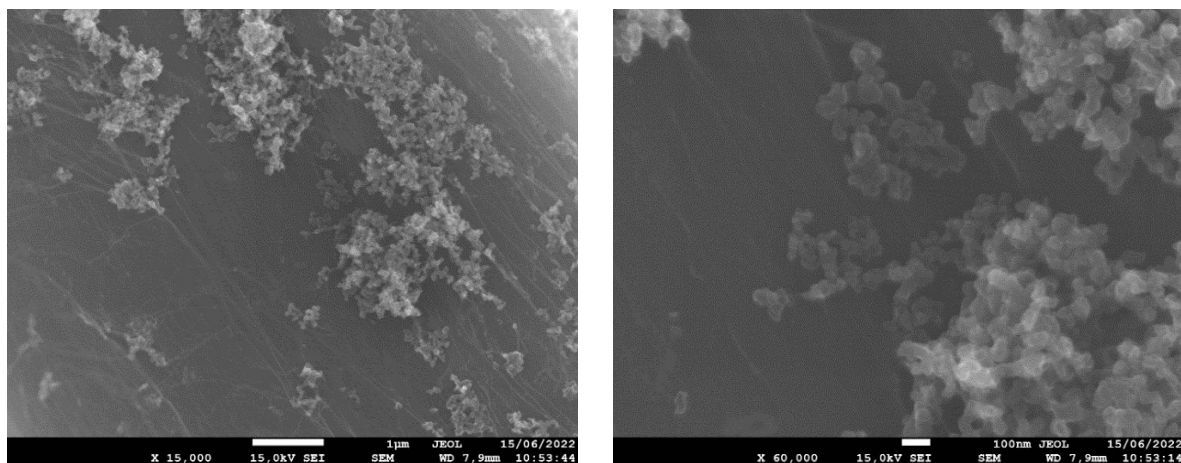


Figure S12. SEM images of Mn@Terpy-COF |NT before CPE.

A)



B)

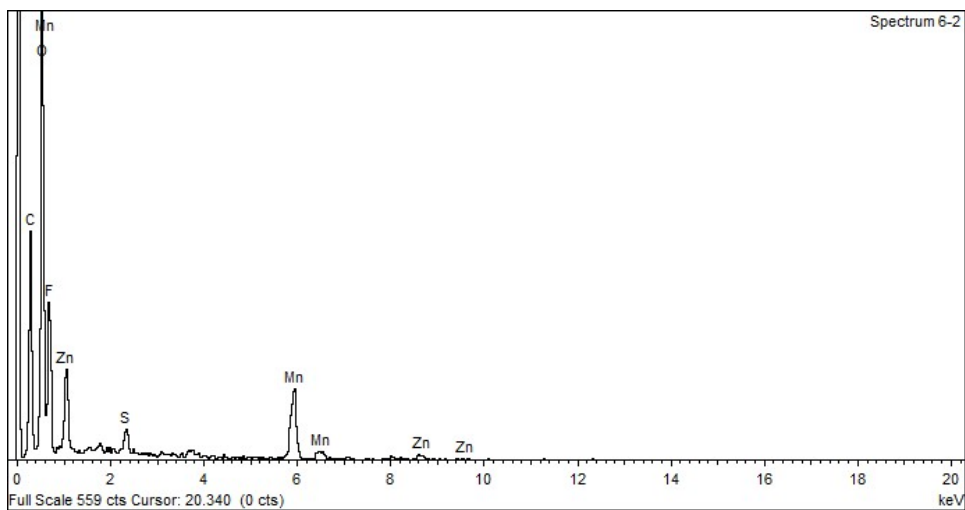
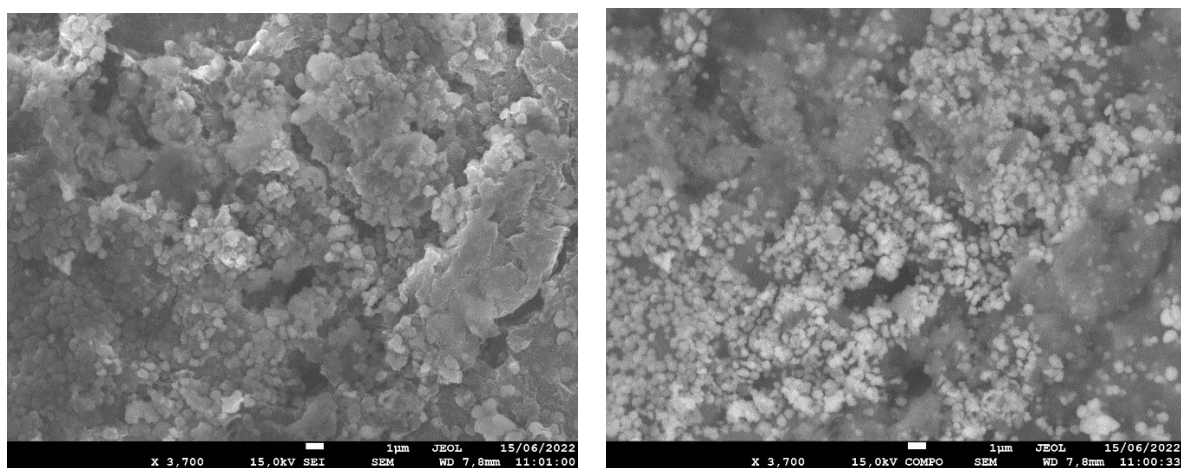


Figure S13. A) SEM images of Mn@Terpy-COF |NT after CPE. B) Secondary electron micrograph (top left), backscatter electron micrograph (top right) and EDS spectra of Mn@Terpy-COF |NT after CPE.

8. THERMOGRAVIMETRIC ANALYSIS (TGA) OF TERPY-COF AND Mn@TERPY-COF

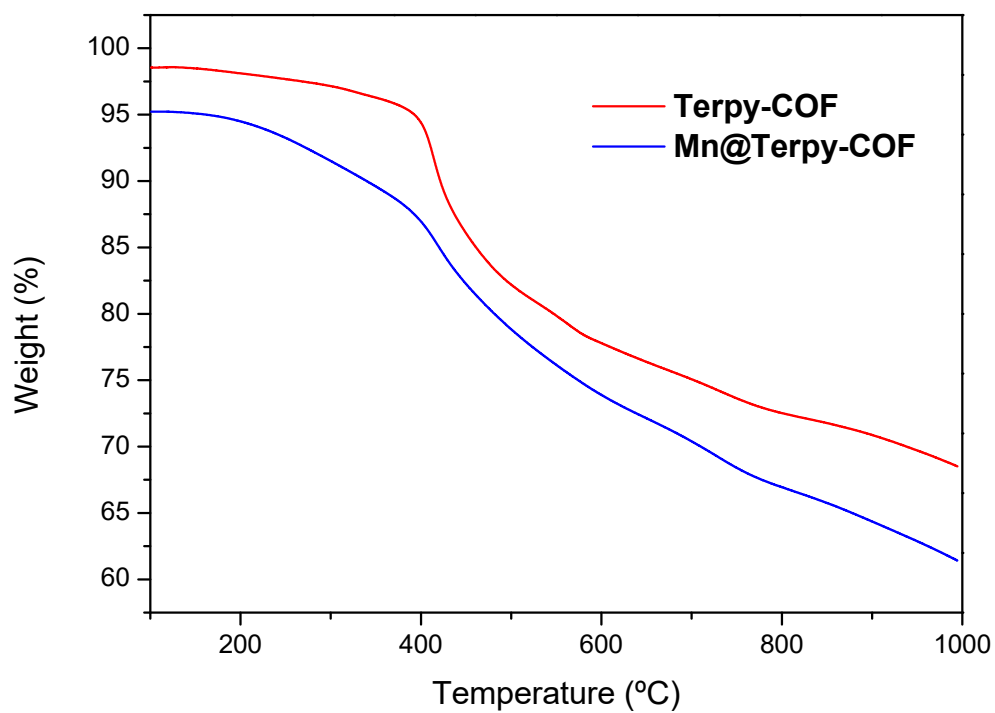


Figure S14. TGA of Terpy-COF (red) and Mn@Terpy-COF (blue).

9. POWDER X-RAY DIFRACTION OF TERPY-COF AND Mn@TERPY-COF

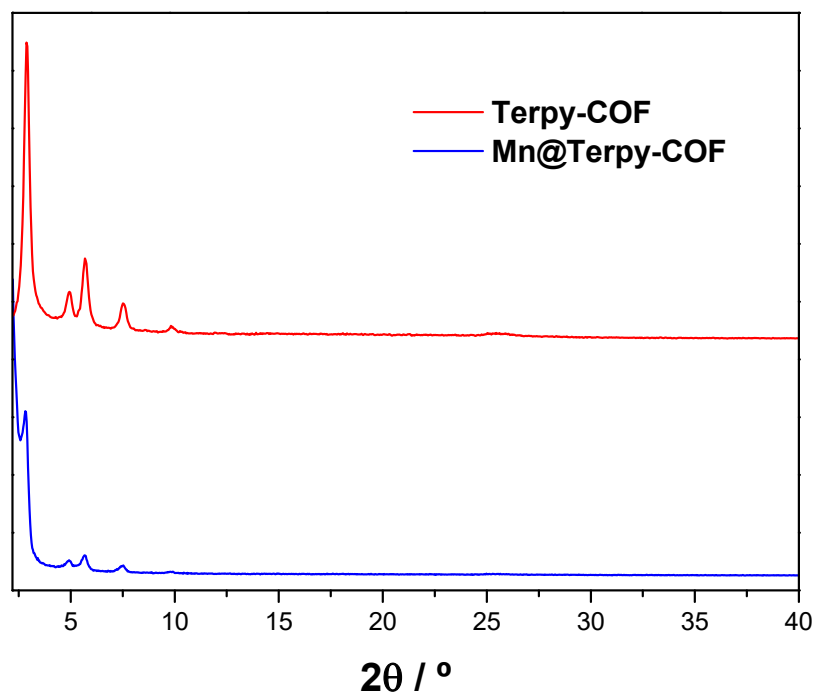


Figure S15. Comparative PXRD spectra of **Terpy-COF** (red) and **Mn@Terpy-COF** (blue).

10. XPS SPECTRA

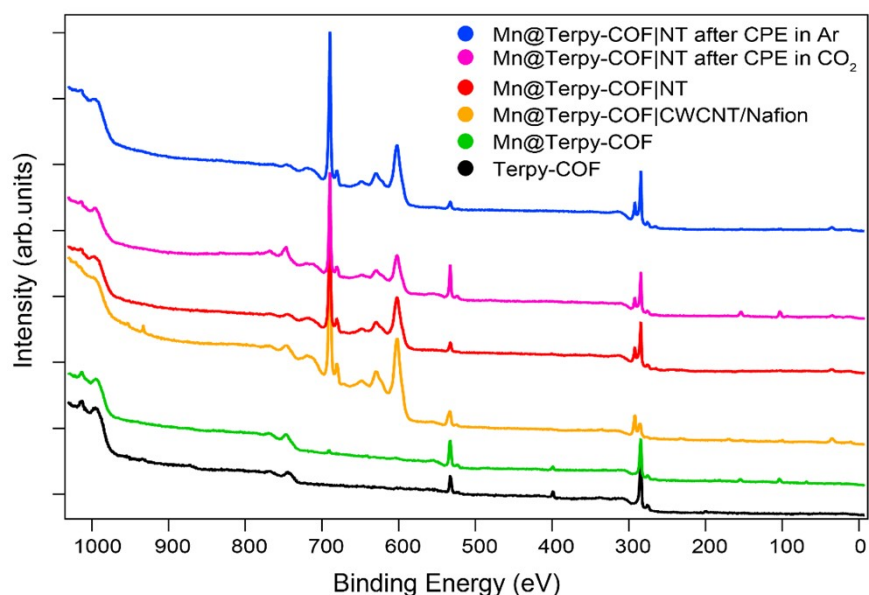


Figure S16. XPS general spectra for **Terpy-COF** (black), **Mn@Terpy-COF** (green), **Mn@Terpy-COF/CWCNT/Nafion** (orange), **Mn@Terpy-COF|NT** before CPE (red), **Mn@Terpy-COF|NT** after CPE (pink) **Mn@Terpy-COF|NT** after CPE under argon (blue). Main peaks are identified. The photon energy used corresponds to Mg K α , $h\nu=1253.6$ eV.

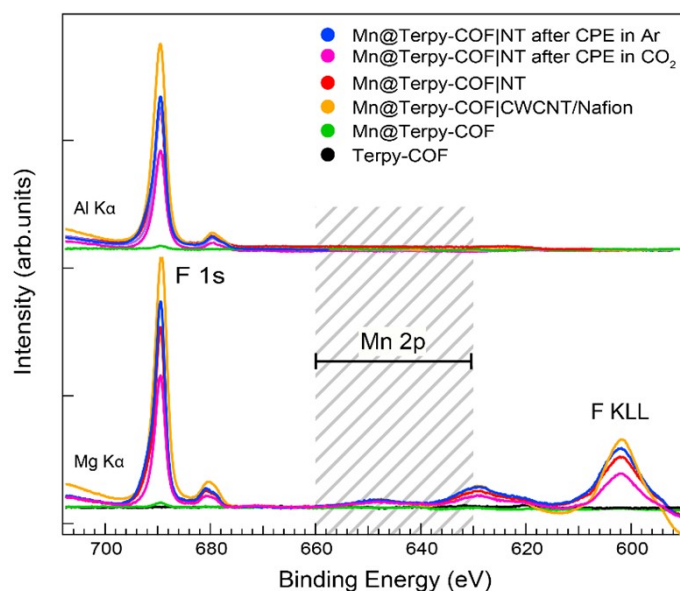


Figure S17. XPS of the binding energy region 700-590 eV measured with Mg K α (1253.6 eV) and Al K α (1486.6 eV), as indicated in the figure. Peaks are identified as F 1s, F KLL (Auger, for Mg K α), Mn 2p and Mn LMM (Auger near Mn 2p for spectra obtained with Mg K α photon source, not observed). Colours correspond with **Terpy-COF** (black), **Mn@Terpy-COF** (green), **Mn@Terpy-COF/CWCNT/Nafion** (orange), **Mn@Terpy-COF|NT** before CPE (red), **Mn@Terpy-COF|NT** after CPE (pink) **Mn@Terpy-COF|NT** after CPE under argon (blue).

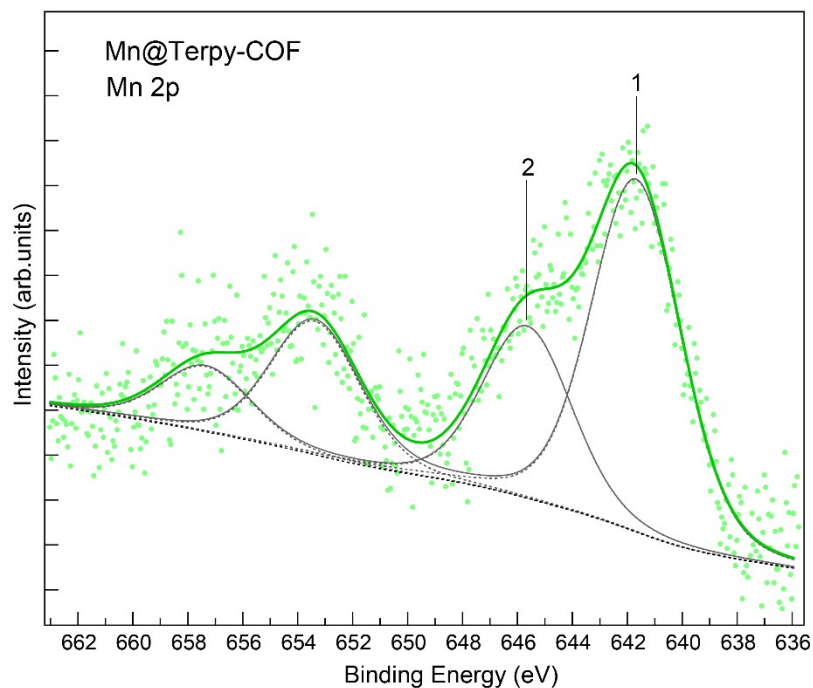


Figure S18. Ampliation and deconvolution of XPS Mn 2p of **Mn@Terpy-COF**. Measured with Al K α (1486.6 eV)

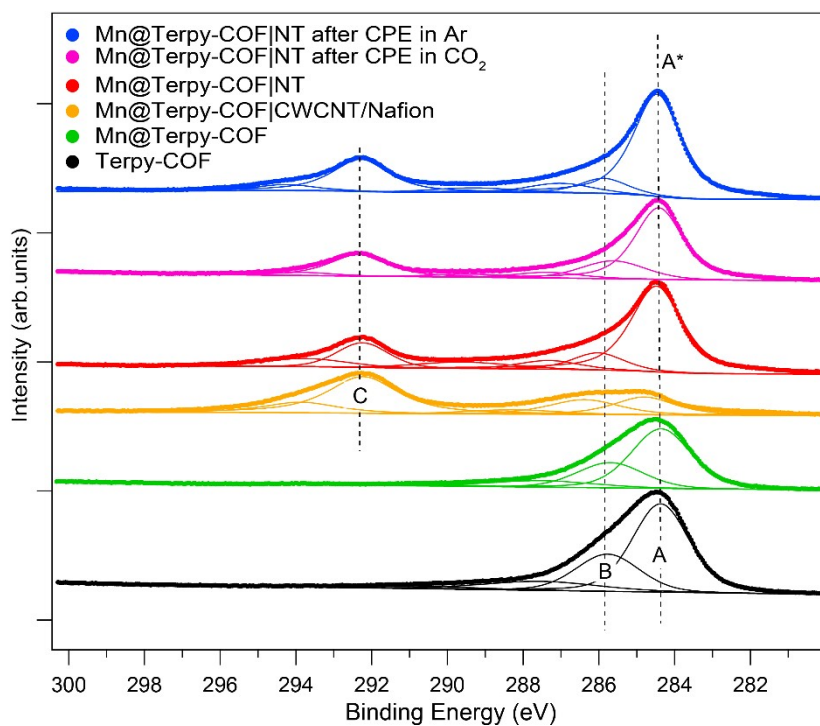


Figure S19. C 1s and deconvolution of relevant peaks of **Terpy-COF** (black), **Mn@Terpy-COF** (green), **Mn@Terpy-COF/CWCNT/Nafion** (orange), **Mn@Terpy-COF|NT** before CPE (red), **Mn@Terpy-COF|NT** after CPE (pink) **Mn@Terpy-COF|NT** after CPE under argon (blue). Measured with Mg K α (1253.6 eV).

Table S1. Positions of binding energy (eV) of main components. % area of each component appear between brackets.

	C 1s			N 1s			Mn 2p		F 1s
	A	B	C	A	B	C	1	2	
Terpy-COF	284.35	285.9		398.5 (78%)	399.9 (14%)	401.5 (8%)	-		-
Mn@Terpy-COF	284.35	285.9		398.5 (65%)	399.8 (27%)	401.8 (8%)	642 (67%)	645.9 (33%)	690.4
Mn@Terpy-COF NT after CPE in CO₂	284.5	285.8	292.3						689.5
Mn@Terpy-COF NT after CPE in Ar	284.5	285.8	292.3						689.45

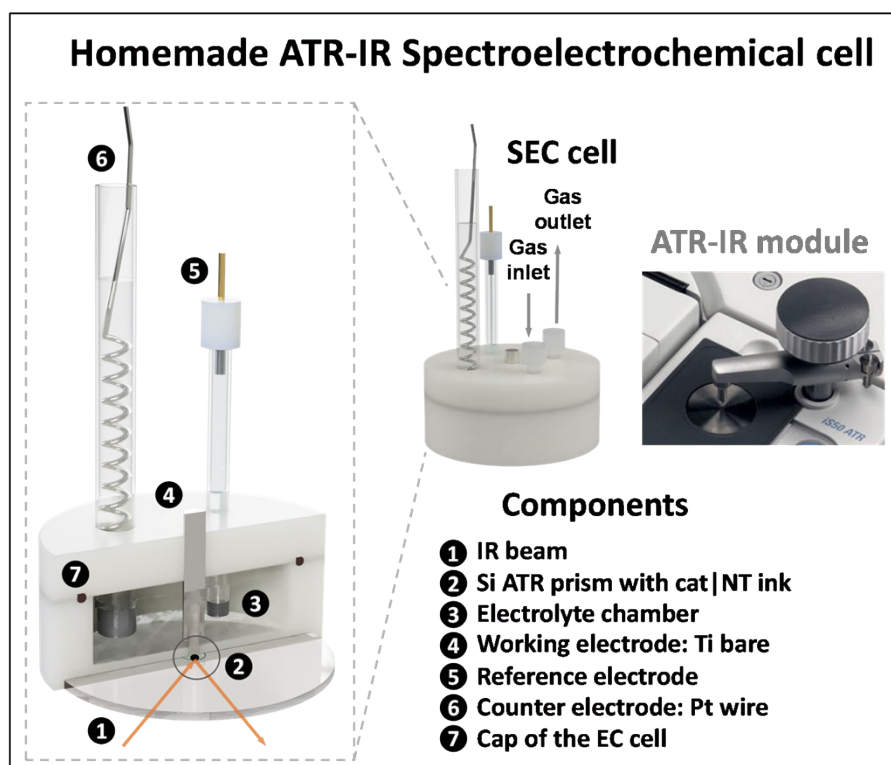


Figure S20. Homemade ATR-FT-IR-SEC.

11. CPE EXPERIMENTS

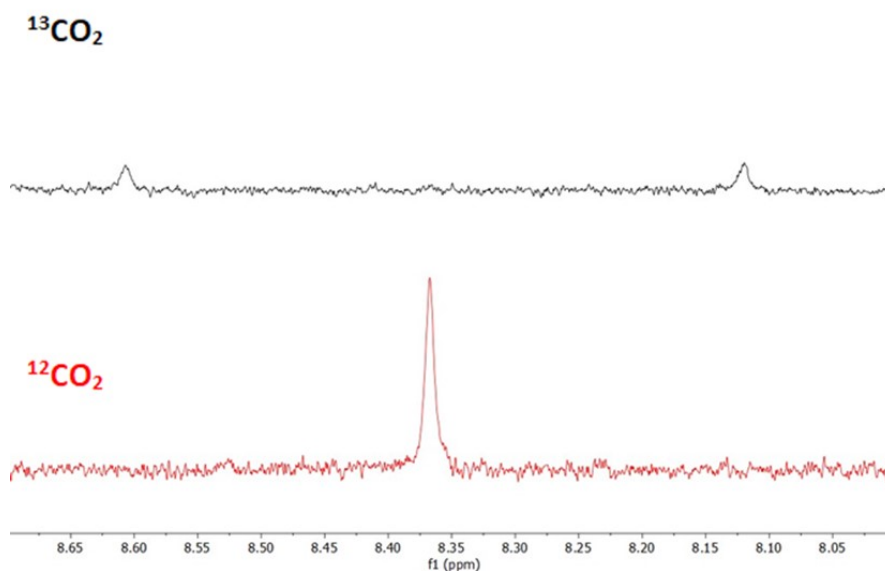


Figure S21. Isotopic labeling control potential electrolysis (CPE) experiment. $^1\text{H-NMR}$ spectra (400 MHz, D_2O) on 600 μL electrolyte aliquot after 800 s of CPE in 0.2 M K_2SO_4 / 0.1M $\text{K}_2\text{B}_4\text{O}_7$ under $^{13}\text{CO}_2$ (top) and under $^{12}\text{CO}_2$ (bottom). The CPE experiments were performed with $\text{CO}_{\text{FtpyMn}} | \text{NT}$ at -1.4 V vs SCE under CO_2 and $^{13}\text{CO}_2$.

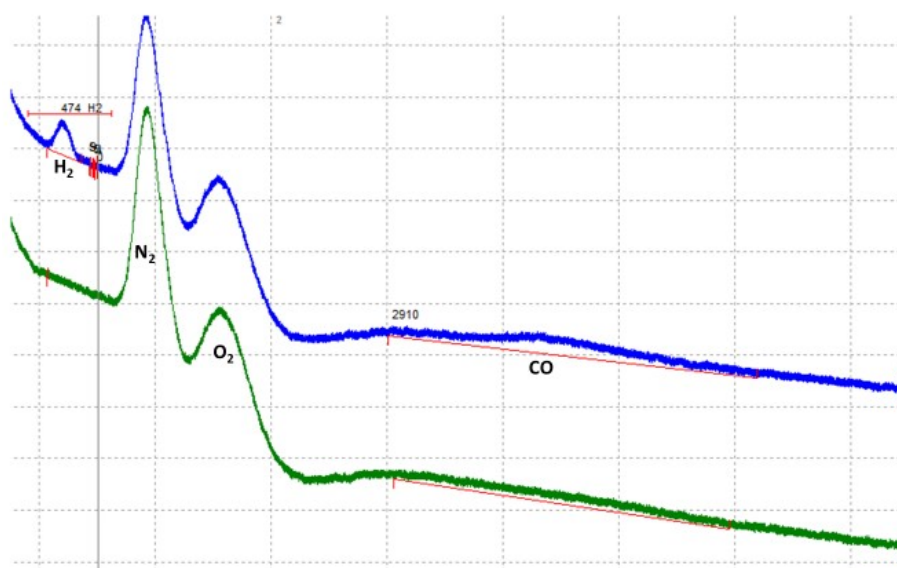


Figure S22. Chromatograms recorded during Controlled Potential Electrolysis (CPE) at $E = -1.4$ V vs SCE to show the appearance of CO and H_2 peaks. The green trace represents $t = 0$ s while the blue trace corresponds to $t = 600$ s.

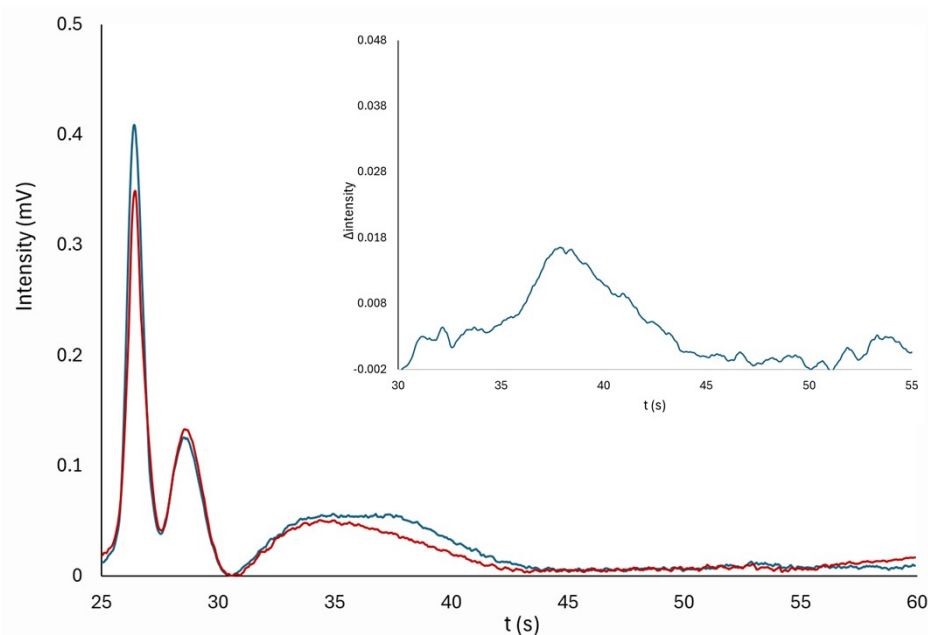


Figure S23: Overlapping of chromatograms recorded after 600 s of CPE at -1.4 V vs SCE (blue) and at the beginning of the experiment ($t = 0$ s, red) showing the appearance of the CO peak. **Inserted Figure** Subtraction of chromatograms at $t = 600$ s and $t = 0$ s was used to calculate the integral of CO peaks.

12. CV OF Mn@TERPY-COF|NT

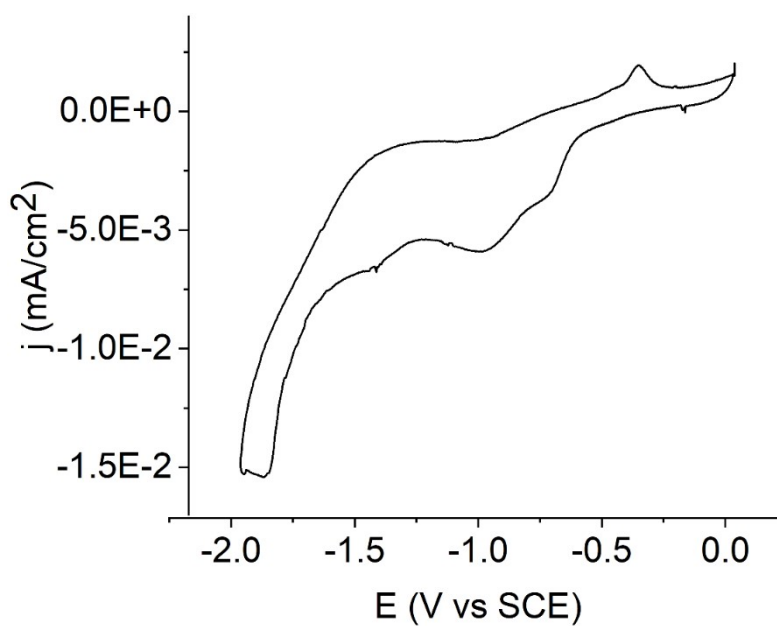


Figure S24: Cyclic voltammogram of Mn@Terpy-COF|NT in dry CH_3CN (0.2 M TBAPF_6) under Ar.

13. ATR SPECTRA OF TERPY-COF AND Mn@TERPY-COF

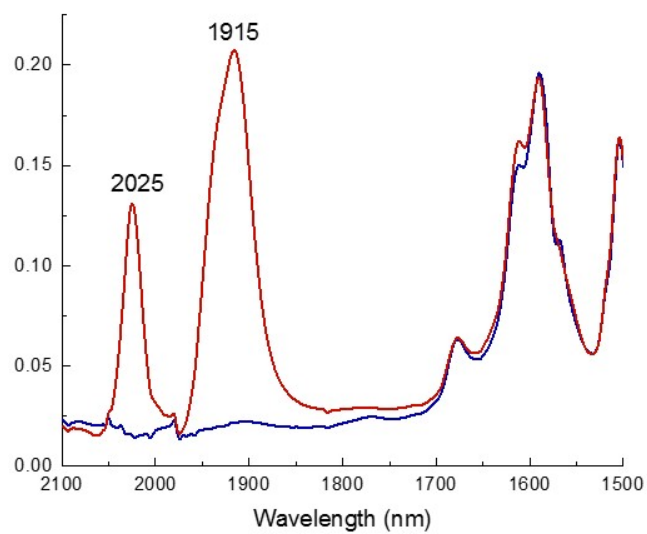


Figure S25. ATR spectra of Terpy-COF (blue) and Mn@Terpy-COF (red). $\nu_{(\text{CO})}$ at 2025 and 1915 cm^{-1} .

14. REFERENCES

- 1 H. Xu, J. Gao and D. Jiang, *Nat. Chem.*, 2015, **7**, 905–912.
- 2 Z. Zhou, G. H. Sarova, S. Zhang, Z. Ou, F. T. Tat, K. M. Kadish, L. Echegoyen, D. M. Guldi, D. I. Schuster and S. R. Wilson, *Chem. - A Eur. J.*, 2006, **12**, 4241–4248.
- 3 M. J. Frisch, G. W. Trucks, H. B. Schlegel, G. E. Scuseria, M. a. Robb, J. R. Cheeseman, G. Scalmani, V. Barone, G. a. Petersson, H. Nakatsuji, X. Li, M. Caricato, a. V. Marenich, J. Bloino, B. G. Janesko, R. Gomperts, B. Mennucci, H. P. Hratchian, J. V. Ortiz, a. F. Izmaylov, J. L. Sonnenberg, Williams, F. Ding, F. Lipparini, F. Egidi, J. Goings, B. Peng, A. Petrone, T. Henderson, D. Ranasinghe, V. G. Zakrzewski, J. Gao, N. Rega, G. Zheng, W. Liang, M. Hada, M. Ehara, K. Toyota, R. Fukuda, J. Hasegawa, M. Ishida, T. Nakajima, Y. Honda, O. Kitao, H. Nakai, T. Vreven, K. Throssell, J. a. Montgomery Jr., J. E. Peralta, F. Ogliaro, M. J. Bearpark, J. J. Heyd, E. N. Brothers, K. N. Kudin, V. N. Staroverov, T. a. Keith, R. Kobayashi, J. Normand, K. Raghavachari, a. P. Rendell, J. C. Burant, S. S. Iyengar, J. Tomasi, M. Cossi, J. M. Millam, M. Klene, C. Adamo, R. Cammi, J. W. Ochterski, R. L. Martin, K. Morokuma, O. Farkas, J. B. Foresman and D. J. Fox, 2016, Gaussian 16, Revision C.01, Gaussian, Inc., Wallin.
- 4 Y. Zhao and D. G. Truhlar, *Theor. Chem. Acc.*, 2008, **120**, 215–241.
- 5 P. C. Hariharan and J. A. Pople, *Theor. Chim. Acta*, 1973, **28**, 213–222.
- 6 W. J. Hehre, R. Ditchfield and J. A. Pople, *J. Chem. Phys.*, 1972, **56**, 2257–2261.
- 7 M. M. Francl, W. J. Pietro, W. J. Hehre, J. S. Binkley, M. S. Gordon, D. J. DeFrees and J. A. Pople, *J. Chem. Phys.*, 1982, **77**, 3654–3665.
- 8 P. Giannozzi, S. Baroni, N. Bonini, M. Calandra, R. Car, C. Cavazzoni, D. Ceresoli, G. L. Chiarotti, M. Cococcioni, I. Dabo, A. Dal Corso, S. de Gironcoli, S. Fabris, G. Fratesi, R. Gebauer, U. Gerstmann, C. Gougoussis, A. Kokalj, M. Lazzeri, L. Martin-Samos, N. Marzari, F. Mauri, R. Mazzarello, S. Paolini, A. Pasquarello, L. Paulatto, C. Sbraccia, S. Scandolo, G. Sclauzero, A. P. Seitsonen, A. Smogunov, P. Umari and R. M. Wentzcovitch, *J. Phys. Condens. Matter*, 2009, **21**, 395502.
- 9 J. P. Perdew, K. Burke and M. Ernzerhof, *Phys. Rev. Lett.*, 1996, **77**, 3865–3868.
- 10 S. Grimme, J. Antony, S. Ehrlich and H. Krieg, *J. Chem. Phys.*, 2010, **132**, 154104.
- 11 A. M. Rappe, K. M. Rabe, E. Kaxiras and J. D. Joannopoulos, *Phys. Rev. B*, 1990, **41**, 1227–1230.
- 12 N. Mounet and N. Marzari, *Phys. Rev. B*, 2005, **71**, 205214.
- 13 J. D. Pack and H. J. Monkhorst, *Phys. Rev. B*, 1977, **16**, 1748–1749.

- 14 J. K. Nørskov, J. Rossmeisl, A. Logadottir, L. Lindqvist, J. R. Kitchin, T. Bligaard and H. Jónsson, *J. Phys. Chem. B*, 2004, **108**, 17886–17892.
- 15 I. C. Man, H.-Y. Su, F. Calle-Vallejo, H. A. Hansen, J. I. Martínez, N. G. Inoglu, J. Kitchin, T. F. Jaramillo, J. K. Nørskov and J. Rossmeisl, *ChemCatChem*, 2011, **3**, 1159–1165.
- 16 E. Cancès, B. Mennucci and J. Tomasi, *J. Chem. Phys.*, 1997, **107**, 3032–3041.
- 17 M. Schmid, H. P. Steinrück and J. M. Gottfried, *Surf. Interface Anal.*, 2014, **46**, 505–511.